Supplementary Material

This work reevaluates measurements from 11 recent cruises, and their locations are shown below.

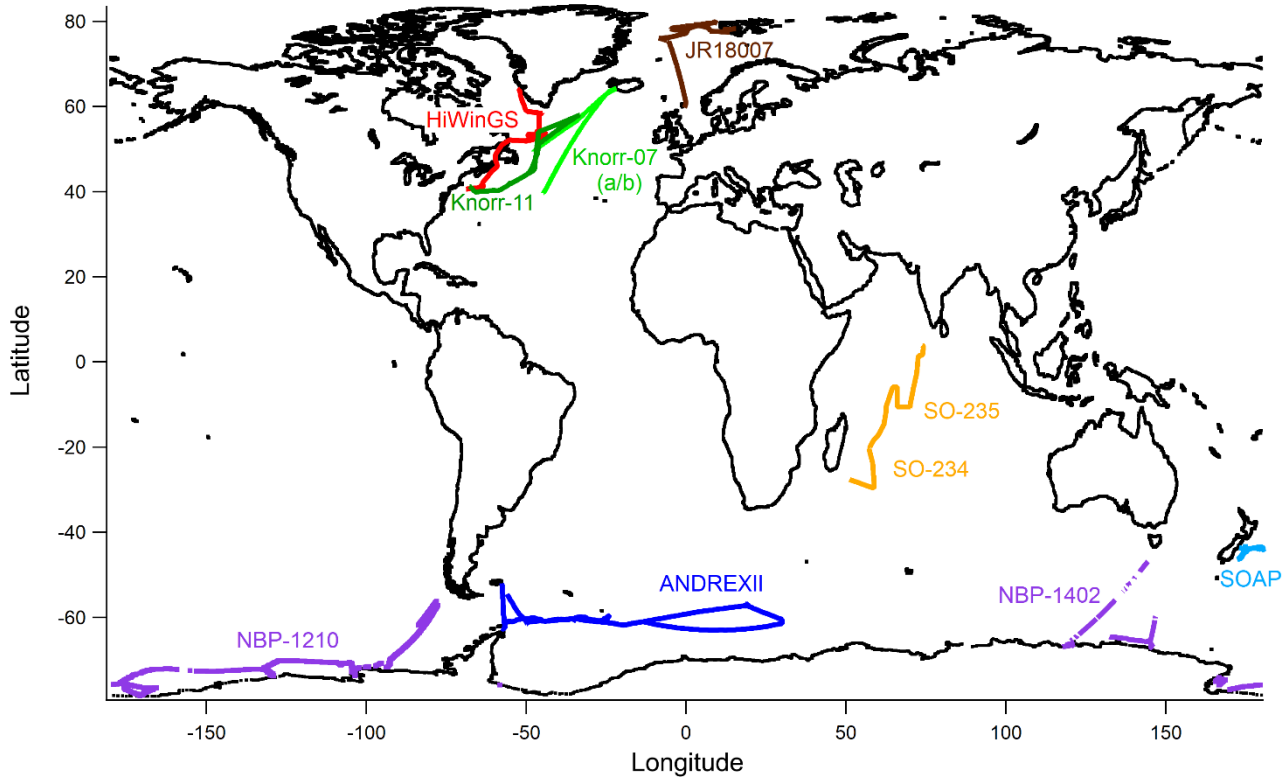

Supplementary Figure 1. Cruise tracks of the 11 research cruises analyzed.

Diurnal warm layer

Woolf et al. (2016) discussed the effects of near surface temperature gradients (namely the cool skin effect and the diurnal warm layer effect) on the calculation of CO_2 flux. We have already accounted for the ocean cool skin in Eq. 2 by using the COARE 3.5 model. While it has been suggested (Holding et al. 2019) that satellite observations may be the best source of subskin temperature (to account for the presence of diurnal warm layer), this does not seem to be the most suitable approach for evaluating cruise data because of the limited number of data matchup. Instead, we assess the significance and prevalence of diurnal warm layer using in-situ observations from the HiWinGS (North Atlantic) and SO GasEx (Southern Ocean) projects. Specifically, this is based on temperature measurements at ca. 1 cm depth using a floating thermistor (aka the NOAA "sea snake"). As shown in Supplementary Figures 2 and 3, across most wind speeds the difference between the sea snake (or subskin) temperature and the underway bulk temperature at ca. 5 m depth is on average negligible (within ~0.02 °C). Only during periods of strong solar insolation and fairly low wind speeds were there signs of a weak diurnal warm layer (i.e., subskin temperature > underway temperature, more obvious in SO GasEx). In the 11 cruises analyzed here, only SO-234/235 took place in the tropics, where the diurnal warm layer could be stronger and more prevalent (e.g., Fairall et al. 1996). Thus

we have insufficient information to fully evaluate the diurnal warm layer effect in this set of cruises and choose to neglect it in our analysis.

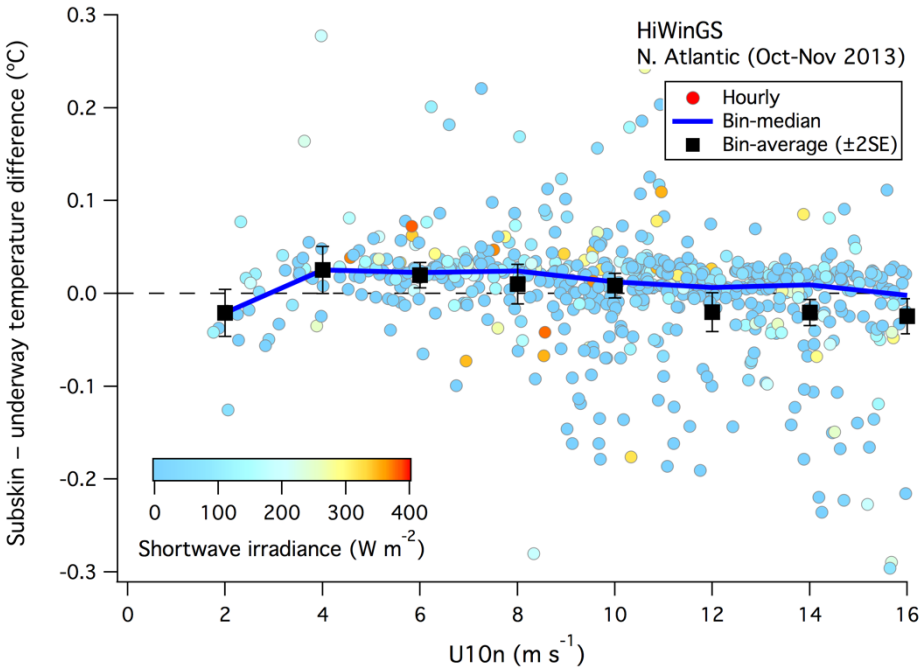

Supplementary Figure 2. Difference between subskin temperature (measured by the NOAA "Seasnake") and underway water temperature during the HiWinGS cruise.

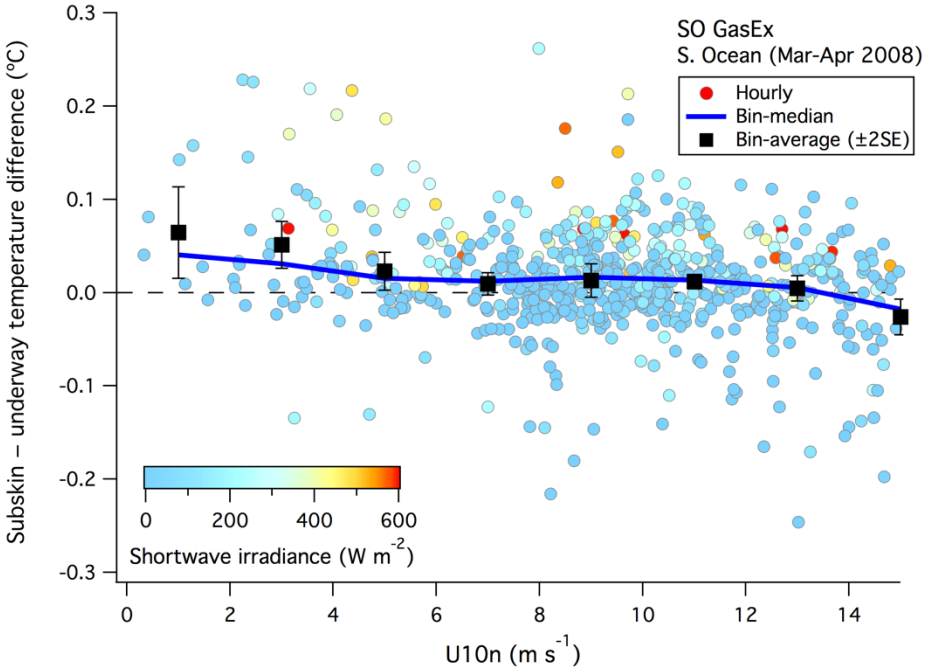

Supplementary Figure 3. Difference between subskin temperature (measured by the NOAA "Seasnake") and underway water temperature during the SO GasEx cruise.

In-situ vs. model winds

EC-derived K_{660} is plotted against in-situ and ECWMF model U_{10n} in Supplementary Figure 4. There is generally greater variability in the K_{660} relationships with model U_{10n} than with in-situ U_{10n} at moderate wind speeds, where most of the observations were made.

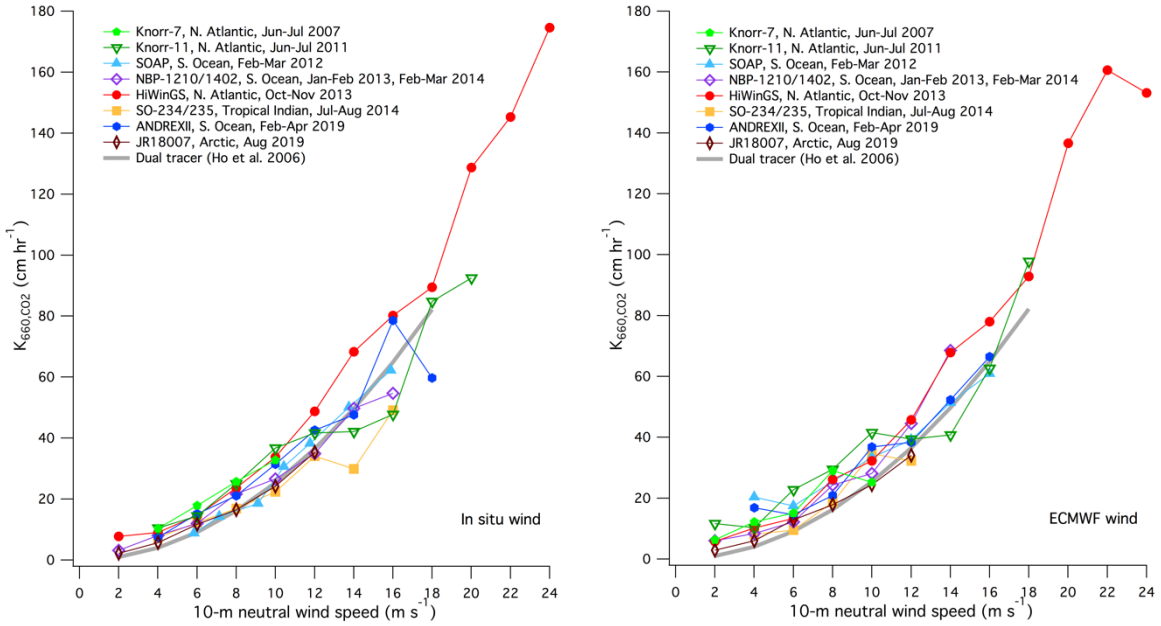

Supplementary Figure 4. K_{660} averaged to bins of in-situ U_{10n} (left) and ECMWF U_{10n} (right). The slightly different distributions of data points within the highest/lowest bins for some cruises are due to the differences between in-situ and model U_{10n}.

Schmidt number normalization at low wind speeds

Supplementary Figure 5 shows K_{660} normalized using a variable Schmidt number exponent (Esters et al. 2017, here limiting n between -2/3 and -1/2) instead of a constant n of -1/2. This result can be compared to Figure 2 in the main paper. At u_* up to 0.9 m s^{-1}, allowing the Schmidt number exponent to vary changes the cruise mean K_{660} slightly: Knorr-07 (+3.1%), Knorr-11 (+1.1%), SOAP (+0.6%), NBP-1210/1402 (+3.5%), HiWinGS (+1.1%), SO-234/235 (-0.7%), ANDREXII (+2.5%), JR18007 (+3.6%). As expected, the largest relative changes occur at low wind speeds and when the water temperature is furthest away from 20º C.

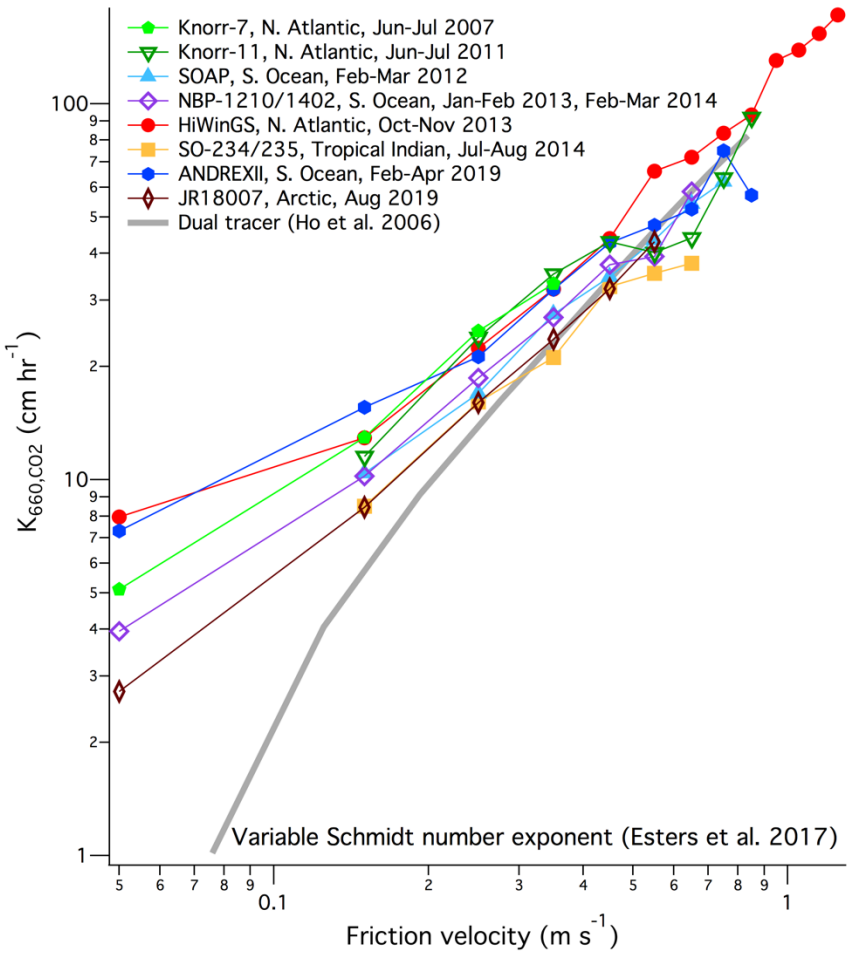

Supplementary Figure 5. K_{660} normalized using a variable Schmidt number exponent.

Relationship between waves and wind

Supplementary Figure 6 shows the very different relationships between significant wave height (H_s) and friction velocity for all the cruises, presumably due to the variable meteorological conditions, sea states, and wind fetches. Also shown is the approximate global average relationship between H_s and u_* from ECMWF ERA5 (0.5°, hourly resolution data; Hersbach et al. 2018), here computed from 12 evenly spaced days in year 2020 (e.g., 1st January, 1st February, 1st March…). The grand average H_s from all the cruises is similar to the global average in low to moderate winds and is slightly lower than the global average in high winds.

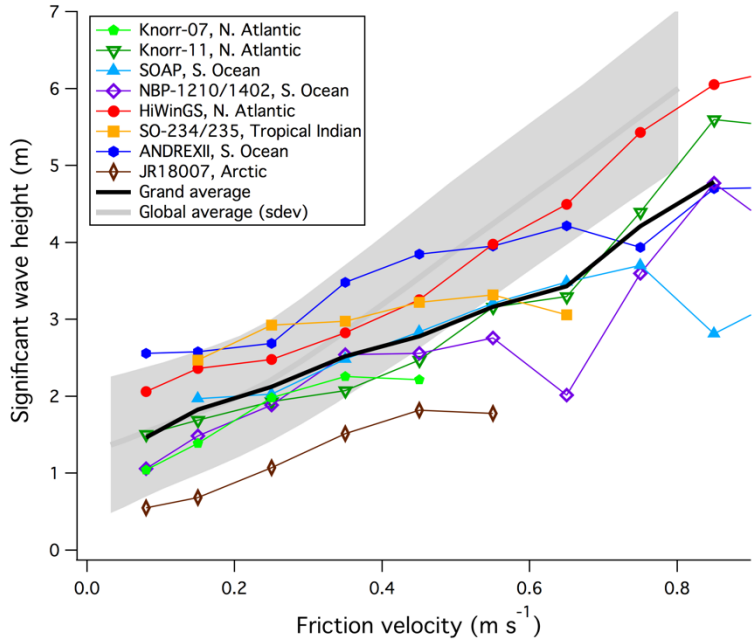

Supplementary Figure 6. Significant wave height averaged in friction velocity bins for the individual cruises, the grand average H_s from all the cruises, as well as the approximate global average H_s (shading represents one standard deviation).

Supplementary Data

Reanalyzed hourly data in air-sea CO_2 exchange, supporting in-situ measurements, as well as ECMWF wave data for each cruise can be found in the supplement.

References

Fairall, C.W., Bradley, E.F., Godfrey, J. S., Wick, G. A., Edson, J. B., and Young, G. S.: Cool skin and warm layer effects on the sea surface temperature. J. Geophys. Res., 101, 1295–1308, 1996.

Hersbach, H., Bell, B., Berrisford, P., Biavati, G., Horányi, A., Muñoz Sabater, J., Nicolas, J., Peubey, C., Radu, R., Rozum, I., Schepers, D., Simmons, A., Soci, C., Dee, D., Thépaut, J-N.: ERA5 hourly data on single levels from 1979 to present. Copernicus Climate Change Service (C3S) Climate Data Store (CDS). (Accessed on < 15-Nov-2021 >), 10.24381/cds.adbb2d47, 2018.

Ho, D. T., Law, C. S., Smith, M. J., Schlosser, P., Harvey, M., and Hill, P.: Measurements of air–sea gas exchange at high wind speeds in the Southern Ocean: Implications for global parameterizations, Geophys. Res. Lett., 33, L16611, https://doi.org/10.1029/2006GL026817, 2006.

Holding, T., Ashton, I. G., Shutler, J. D., Land, P. E., Nightingale, P. D., Rees, A. P., Brown, I., Piolle, J.-F., Kock, A., Bange, H. W., Woolf, D. K., Goddijn-Murphy, L., Pereira, R., Paul, F., Girard-Ardhuin, F., Chapron, B., Rehder, G., Ardhuin, F., and Donlon, C. J.: The FluxEngine air–sea gas flux toolbox: simplified interface and extensions for in situ analyses and multiple sparingly soluble gases, Ocean Sci., 15, 1707–1728, https://doi.org/10.5194/os-15-1707-2019, 2019.